MAGNETIC FIELD SENSING WITH A MINIATURE ELECTRO-OPTIC SENSOR FOR INTERVENTIONAL MAGNETIC RESONANCE IMAGING

Alp A. Derin[1], Abhiram Pulavarthi[1], Jordan L. Edmunds[2], Jack Guida[1], Siddhartha Ghosh[1], and Soner Sonmezoglu[1*]*
[1]Northeastern University, Boston, Massachusetts, USA
[2]University of California, Berkeley, California, USA

ABSTRACT

Technologies that enable precise localization and real-time tracking of interventional devices, such as catheters, under magnetic resonance imaging (MRI) are necessary to guide minimally invasive interventions for high-risk patients. At present, MRI-based catheter tracking relies on passive and active devices. However, current and emerging devices have demonstrated shortcomings due to their poor contrast generation, radiofrequency (RF)-induced heating inside the body or large size. Here, we present an innovative RF magnetic field sensor with a miniature millimeter (mm)-sized probe to allow active catheter tracking for image-guided interventional procedures in 1.5T MRI. The sensor is designed to enable operation with virtually zero probe heat-up inside the body and hence eliminate the heating safety risk. We believe this work would open the door to the realization of sensors with sub-mm-scale probes that can enable safer, minimally invasive MRI-guided catheter-based interventions and thus improve patient outcomes.

KEYWORDS

Interventional MRI, Active Tracking, Optical Microresonator, Electro-Optic Sensor, RF Magnetic Field

INTRODUCTION

Accurate real-time tracking of catheters with clinical imaging modalities is essential to guide and transform targeted interventions for patients with major diseases such as cardiovascular disease. X-ray fluoroscopy is currently the predominant imaging modality that allows in vivo tracking of tungsten or $BaSO_4$-doped catheters in real time [1]. However, X-ray fluoroscopy suffers from low soft tissue contrast [2] and hence requires expert practitioners to determine the catheter position and orientation relative to anatomical structures. In addition, X-ray ionizing radiation raises health and safety concerns for patients and medical professionals during medical procedures.

Unlike X-ray fluoroscopy, magnetic resonance imaging (MRI) has shown the ability to provide high soft tissue contrast without ionizing radiation. MRI-based catheter tracking in the body has been demonstrated by using passive and active devices. Existing passive devices often formed by magnetic materials suffer from orientation-dependent artifacts and poor contrast [3], limiting their deployment in clinical practice. On the other hand, most existing active devices rely on RF receivers based on either coil [4] or loop antennas [5] to detect MRI-induced RF magnetic fields from the tissue and transmit the detected signals to the MR scanner outside the body to enable localization. Although this approach provides relatively accurate localization and tracking of the catheters, these active devices have an inherent limitation of RF-induced heating inside the body. This arises because these devices convey the detected RF signals on long electrical cables to the MRI system [6]. Several methods, including parallel RF transmission [7] and saline coolant flow through the catheter [8], have been demonstrated to reduce RF heating but with minimal success.

The RF-induced heating issue led to the development of active tracking devices based on the transduction of an electrical RF signal in the optical domain. These devices rely on either an optoelectronic circuit [9] or a Fiber Bragg grating (FBG) modulator [10] to convert the RF signal to an optical signal and carry the resulting signal on a compact optical fiber instead of electrical cables, eliminating the RF heating safety risk. However, these devices are currently limited by localized tissue heating due to circuit power dissipation or large size, frequently causing post-operative complications.

Here, we present a magnetic field sensor for tracking catheter position in real-time during interventional MRI, showing promise of avoiding the drawbacks of the active devices mentioned above. The sensor core element is a mm-scale probe that incorporates a coil loop antenna and a microfabricated optical microresonator (OMR). The OMR is a high-Q resonant cavity based on piezoelectric actuation, operating as an optical intensity modulator. In operation, the antenna detects and converts the MRI-induced RF magnetic field from the tissue to an electrical signal, which in turn modulates the OMR. Therefore, the magnetic field is transformed into an electrical and then an optical signal. The high-Q OMR greatly enhances the signal-to-noise ratio (SNR) of the detected RF signals; this enables the miniaturization of the antenna and, hence, the probe size. A single-mode fiber coupled to the OMR carries the optical signal, in which the probe position information is encoded, to a module outside the body. Compared to existing active tracking approaches [4-10], our design approach allows the sensor to operate with virtually zero probe power/heat-up inside the body and allows miniaturization of the probe diameter to less than 2mm while achieving a competitive resolution of 20pT/√Hz. These unique features provide potential capabilities for use in interventional MRI procedures with minimal safety risk and tissue invasiveness.

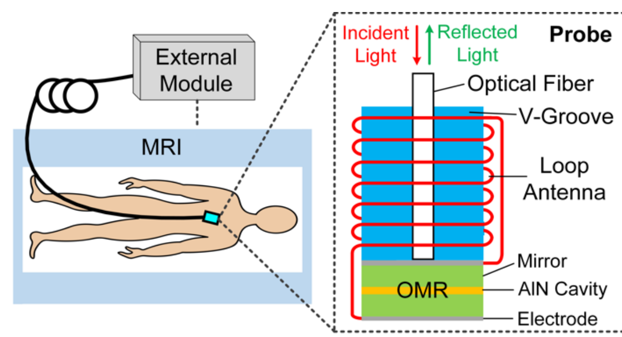

Figure 1: Schematic of the RF magnetic field sensor for use in interventional MRI. The inset shows the probe details. The probe is formed by combining a loop antenna and an optical microresonator (OMR) coupled to a V-groove fiber.

RF MAGNETIC FIELD SENSOR

Operating principle of the sensor. The magnetic field sensor combines a miniature electro-optic probe with a module outside the body (Fig. 1). The probe is formed by a loop coil antenna, an optical microresonator (OMR), and a V-groove fiber. In operation, the loop coil antenna receives the magnetic field component of the RF field emitted by the nearby hydrogen atoms in tissue in MRI and produces an RF voltage due to Faraday's law of induction. The antenna is electrically connected to the high-Q OMR (Fig. 2), such that the induced RF voltage on the antenna modulates the OMR resonant wavelength (λ_{res}). This modulation results in a shift in the reflectance (R) spectra and, hence, a change in light intensity (P_{out}) reflected off the OMR. To maximize the modulation depth (ΔR) and hence the SNR of the RF signal, the OMR is operated with an incident light wavelength (λ_{in}) at the maximum slope of its R curve. This electro-optic transduction enables the transmission of the magnetic field-modulated optical signal on a single optic fiber. In our probe, the V-groove fiber is coupled to the OMR to carry the RF signal encoded in the optical domain to an optoelectronic circuit in the external module for data decoding and further MRI integration.

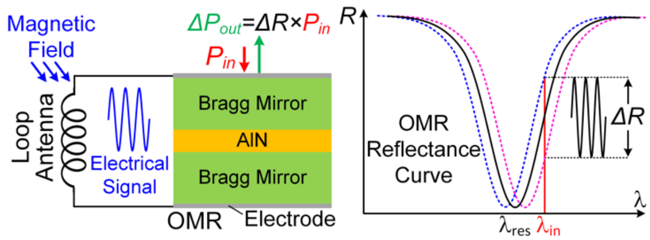

Figure 2: Electro-optic transduction, enabled by an OMR operated with an incident light wavelength λ_{in} at the steepest slope of the R curve to maximize sensitivity. An electrical signal from the antenna causes a shift in the OMR R spectra (dashed lines), modulating the reflected light intensity.

Electro-optic probe design and manufacturing. A miniature electro-optic probe is enabled by the compact integration of a loop coil antenna, the OMR, and the V-groove fiber, in which the antenna mainly sets the probe size. In this work, we used a 14-turn coil antenna with a 1.8mm diameter and a 6mm length. This antenna size was chosen to maintain a reasonable trade-off between its magnetic field sensitivity and the impact on the probe size. In our probe, the coil dimensions can be reduced to 1.5mm in diameter, limited by the V-groove size, but at the expense of reduced sensitivity.

The OMR is designed to operate as a reflective optical intensity modulator, requiring a narrowband laser source for efficient electro-optic transduction of an electrical signal from the loop coil antenna. The OMR is a resonant cavity formed by a piezoelectric Aluminum Nitride (AlN) active layer between two highly reflective distributed Bragg reflector (DBR) mirrors, depicted in our prior work [11]. The device operates with a laser wavelength λ_{in} where the reflectance (R) slope is the steepest near the resonance wavelength λ_{res} (Fig. 2). A voltage (V_{in}) applied across the device electrodes induces an electric field inside the AlN active layer that causes it to change its thickness due to piezoelectric effect, resulting in a shift in the λ_{res} and, hence, a modulation in the R. The modulation depth (ΔR) can be estimated by [12]:

$$\Delta R = \beta \cdot V_{in} \tag{1}$$

$$\beta \approx \frac{3\sqrt{3}}{4} \cdot \frac{R_{max} \cdot Q}{t} \cdot \left(d_{33} + \frac{1}{2}\, n_0{}^2 r_{33} \right) \tag{2}$$

Here, β is the OMR modulation gain, R_{max} is the resonant dip amplitude, Q and t are the device quality factor and the cavity layer thickness, d_{33} is the piezoelectric coefficient, and n_0 and r_{33} are the AlN film unperturbed refractive index and Pockels coefficient. The OMR operated with a light intensity P_{in} exhibits a relative change in the reflected light intensity, $\Delta P_{out} = \Delta R \times P_{in}$.

The OMR was fabricated on a bare p-Si wafer using standard microfabrication techniques. Briefly, the fabrication steps (Fig. 3) include (1) the deposition of an antireflection coating (ARC) layer of 50nm titanium (Ti) and 200nm amorphous Si (α-Si), (2) the deposition of DBRs consisting of nine quarter-wavelength layers of alternating 90nm α-Si and 240nm silicon dioxide (SiO_2), (3) the sputtering of a 310nm-thick AlN active layer, (4) the lithographic patterning and etching of the top mirror and the AlN layer, (5) the sputtering of 10nm Ti/100nm Aluminum (Al) on the backside of the wafer to provide electrical contact to the Si substrate and use it as a bottom electrode, (6) the sputtering and lithographic patterning of a 60nm indium tin oxide (ITO) layer to form the transparent top electrode, and (7) the evaporation and patterning of 300nm-thick Al layer on the top wafer surface using a liftoff process to form the bond pads. The fabrication process details can be found in [11].

In our design, the AlN active layer thickness was adjusted to 310nm to operate the OMR at a 1310nm wavelength. This is mainly because operation at wavelengths > 1μm minimizes the absorption of the materials (ITO, α-Si, and SiO_2) used in the microfabrication. However, the Si substrate is transparent at the operating wavelength; this causes some portion of the light incident upon the device to be reflected off the bottom electrode surface, degrading the device's Q-factor and, therefore, modulation gain β. Therefore, we used an ARC on the Si substrate, eliminating the effect of back reflection on OMR performance.

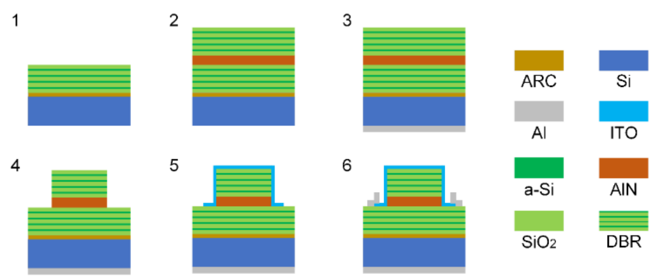

Figure 3: Device fabrication steps. 1. Deposited ARC and bottom DBR mirror on a Si wafer. 2. Deposited AlN active layer and top DBR mirror. 3. Deposited backside Ti/Al ohmic contact. 4. Etched device mesas. 5. Sputtered and patterned ITO layer. 6. Evaporated and patterned Al bond pads.

Fig. 4 shows a photograph of the proof-of-concept sensor probe with the fabricated 5×5mm^2 die containing different-size OMRs. To assemble the probe, the V-groove single-mode fiber was aligned and epoxied onto a 320μm-diameter OMR on the die using UV-curable epoxy (NOA61). Next, the antenna was attached to the OMR using conductive epoxy (MGC 8331) that was cured at room temperature. Multiple different-size OMRs were placed on the same die for their fair performance comparison, limiting the probe size. The size of a die with a single OMR can be reduced to 1×1 mm^2, which would enable a smaller 1.8mm diameter probe, limited by the antenna size.

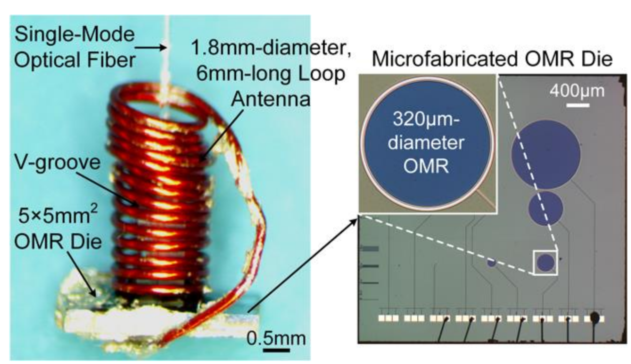

Figure 4: Photograph of the proof-of-concept probe (left), built by integrating a loop antenna and a V-groove fiber with a 320 μm-diameter OMR on the microfabricated die (right).

Fig.5 shows the measured (a) reflectance spectra and (b) optical frequency response of the 320µm-diameter OMR, obtained by using a custom-built reflectometer with a tunable laser (Santec TSL-570) and a power meter (Santec MPM210). The device exhibits a high Q of 1700, yielding a β of 1.5×10^{-3} V^{-1} (calculated using the measured device parameters and Eq. 2). This high β ensures high transduction sensitivity that greatly enhances the RF signal from the antenna and its SNR. This resulting enhancement enables the miniaturization of the antenna and, hence, the probe. The OMR has a bandwidth (BW) of 108MHz, enabling operation inside a 1.5T MRI system with a Larmor frequency of ~64MHz. Note that the OMR operating BW is set by its electrical BW, limited by RC time constant, where R is the resistance from the thin ITO layer, and C is the capacitance from the device layers between its electrodes. This reveals that reducing the device size increases its BW. Although we used a 320µm OMR to prototype the probe in this work, a smaller OMR with a higher BW can be used to enable operation in MRI with magnetic fields > 1.5T.

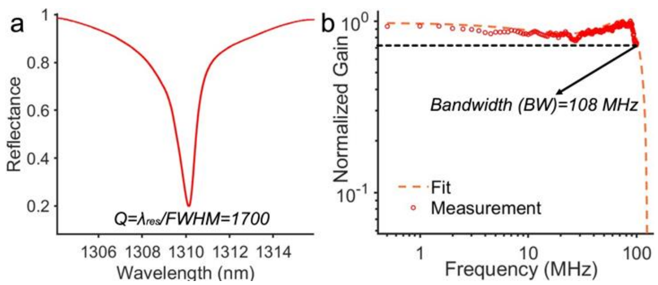

Figure 5: Measured (a) reflectance spectra and (b) frequency response of the 320µm OMR, showing 1700 Q and 108MHz BW.

External module design. An external module (Fig. 6) includes a tunable laser (Santec TSL-570) to interrogate the OMR with the antenna in the probe tip, a circulator (Thorlabs CIR1310) to separate the reflected light from the incident light, and a receiver (Rx) path to read out intensity-modulated optical signals from the probe. In the Rx path, we used an InGaAs balanced photodetector with 350MHz BW (Thorlabs PDB435C) to capture and convert the reflected light into an electrical signal. The resulting RF signal is filtered with a bandpass filter (55-67MHz), phase-shifted, and sent to a DAQ/PC for data analysis and an MRI scanner for tracking the position of the probe tip. Note that the phase shifter is used to remove a constant phase offset of 18° in the sensor output, introduced by the OMR due to its RC-limited bandwidth.

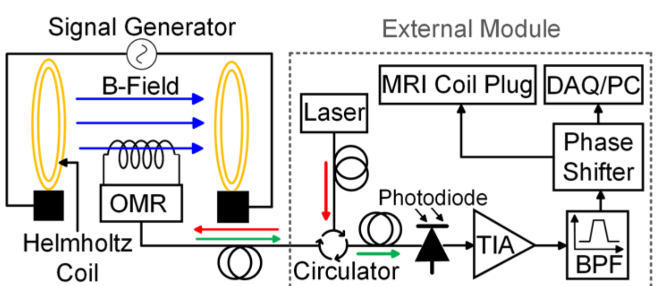

Figure 6: Block diagram of the sensor's external module and the test setup. The setup employs Helmholtz coils that are driven by a signal generator to generate RF magnetic fields.

Sensor performance. The SNR of the magnetic field sensor operated with an incident light power P_{in} is bounded by its magnetic field sensitivity and two main sources of noise – shot noise and TIA noise at the photodetector – which is given by

$$SNR = \frac{S}{N} = \frac{P_{in}\cdot\Delta R^2\cdot\Re}{\overline{i_n^2}\cdot BW} \tag{3}$$

where S and N represent the signal and noise power at the TIA input, and $\Re$ is the responsivity of the photodetector. Eq. 3 reveals that the sensor SNR is dependent on not only the antenna gain (G_{ant}) and the OMR modulation gain (β) through ΔR ($=\beta\cdot G_{ant}\cdot B$, where B is the magnetic field) but also P_{in} and BW. As expected, a larger P_{in} results in a better SNR in the electro-optic sensor with a fixed 108MHz BW.

EXPERIMENT RESULTS

Fig. 6 shows the setup used to characterize the magnetic field sensor. A Helmholtz coil, driven by a signal generator, was used to generate magnetic fields at ~64MHz (1.5T MRI Larmor frequency) [13], simulating RF echoes from the tissue. Experiments were conducted with the sensor operated with an incident light power of 1mW at a wavelength of 1310.5nm (that is, the maximum slope of the R curve (Fig. 5a)). Fig. 7 shows the measured sensor response as a function of the input magnetic field in the range of 50-300nT. The sensor demonstrated 5.2V/mT sensitivity with a linearity of ~0.99.

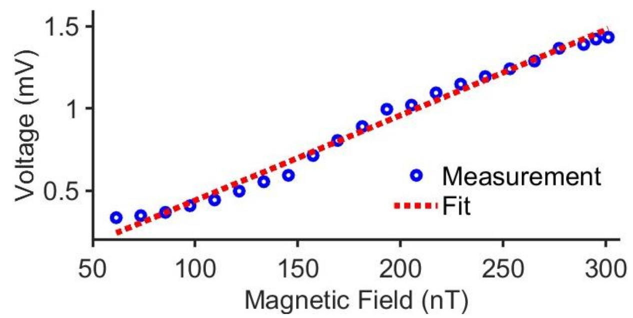

Figure 7: Measured sensor output versus magnetic field at 64MHz. The sensor exhibits a sensitivity of 5.2V/mT.

Fig. 8 shows the sensor input-referred noise spectrum with a 64MHz, 300nT magnetic field input, demonstrating that the sensor achieves an SNR of 43dB and a minimum detectable magnetic field of 20pT/√Hz with 1mW incident optical power and a 108MHz BW. The measured noise floor of the sensor is in excess of the shot noise limit (6.7pA/√Hz) by 7dB, dominated by the TIA noise. Note that we computed the input-referred spectral noise from the data that we collected by dividing the sensor output voltage by its sensitivity.

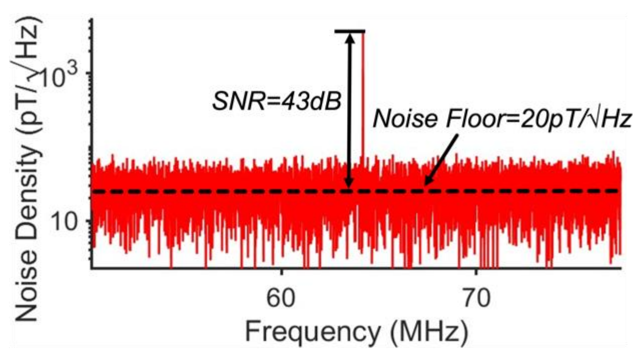

Figure 8: Measured input-referred spectral density with a 300nT, 64MHz magnetic field applied to the sensor. The sensor achieves an SNR of 43dB with a resolution of 20pT/√Hz.

Phase and frequency encoding techniques are used in MRI to detect and track the in vivo position of the catheter tip in the body [13]. These techniques currently rely on an RF field sensor that has a linear phase response and a flat frequency response over a certain BW (e.g., RF signal BW is 100kHz for a 1.2m long 1.5T MRI bore). Therefore, we tested the sensor with a magnetic field input at various phases and frequencies. Fig. 9 shows the measured output responses to a 300nT magnetic field (a) at different phases from 0-60° and (b) at different frequencies from 63.88-64.12MHz. The sensor exhibits a linear phase response with $R^2 > 0.99$ and a uniform frequency response over 240kHz with a standard deviation of 1.4%, verifying the probe's ability to be localized by an MRI scanner.

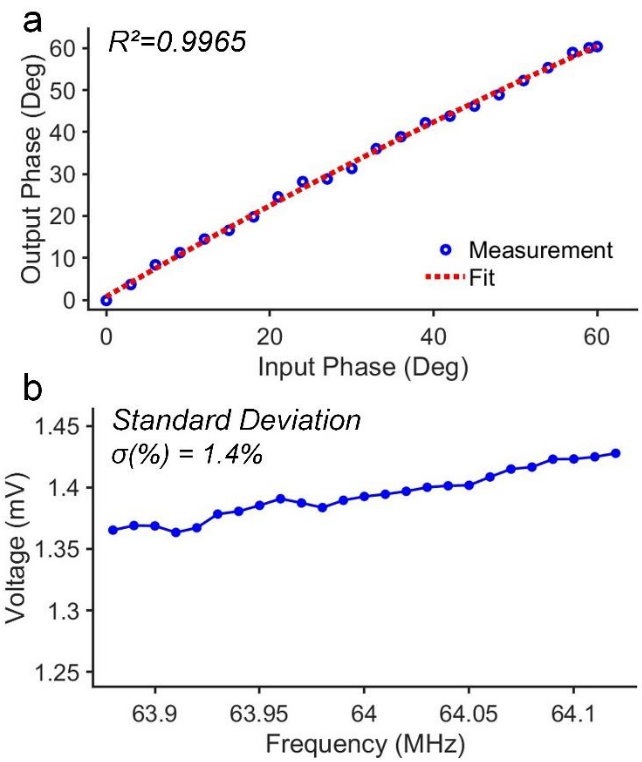

Figure 9: Measured sensor output response to a 300nT magnetic field input with varying (a) phase at 64MHz and (b) frequency at around 64MHz. The sensor exhibits a linear input-output phase relationship and a nearly flat frequency response over 240kHz.

CONCLUSION

We presented an electro-optic RF magnetic field sensor with the potential to enable real-time accurate tracking of the catheter tip in a 1.5T MRI scanner for interventional procedures. The proof-of-concept sensor employs a mm-scale probe and an external module. The probe was enabled by the tight integration of a loop antenna, the high-Q optical microresonator (OMR), and the single-mode optical fiber, in which the OMR die limits the probe size. The sensor was tested with a Helmholtz coil at 64MHz, simulating the RF field of a 1.5T MRI scanner. We demonstrated that the sensor has a 20pT/√Hz resolution, a linear phase response ($R^2 > 0.99$), and a flat frequency response ($\sigma = 1.4\%$); this ensures that the sensor probe is capable of being localized by a 1.5T MRI system. Overall, this work provides a path toward the realization of minimally invasive optical sensors with zero probe heat-up for safer MRI-guided interventions. Future work should focus on sensor performance improvement and probe miniaturization.

ACKNOWLEDGEMENTS

The authors would like to thank Prof. Marvin Onabajo at Northeastern University (NU) for access to lab equipment and the staff of the George J. Kostas Nanomanufacturing Research Center at NU and of the Center for Nanoscale Systems (CNS) at Harvard University for their assistance during device fabrication.

REFERENCES

[1] M. E. M. K. Abdelaziz, L. Tian, M. Hamady, G.-Z. Yang, and B. Temelkuran, 'X-ray to MR: the progress of flexible instruments for endovascular navigation', *Prog. Biomed. Eng.*, vol. 3, no. 3, p. 032004, Aug. 2021.

[2] Y. Ma *et al.*, 'Real-time x-ray fluoroscopy-based catheter detection and tracking for cardiac electrophysiology interventions', *Med. Phys.*, vol. 40, no. 7, p. 071902, 2013.

[3] F. Settecase, A. J. Martin, P. Lillaney, A. Losey, and S. W. Hetts, 'Magnetic Resonance–Guided Passive Catheter Tracking for Endovascular Therapy', *Magn. Reson. Imaging Clin. N. Am.*, vol. 23, no. 4, pp. 591–605, Nov. 2015.

[4] C. L. Dumoulin, S. P. Souza, and R. D. Darrow, 'Real-time position monitoring of invasive devices using magnetic resonance', *Magn. Reson. Med.*, vol. 29, no. 3, pp. 411–415, 1993.

[5] O. Kocaturk *et al.*, 'Active two-channel 0.035″ guidewire for interventional cardiovascular MRI', *J. Magn. Reson. Imaging*, vol. 30, no. 2, pp. 461–465, 2009.

[6] C. J. Bakker *et al.*, 'Visualization of dedicated catheters using fast scanning techniques with potential for MR-guided vascular interventions', *Magn. Reson. Med.*, vol. 36, no. 6, pp. 816–820, 1996.

[7] C. E. McElcheran, B. Yang, K. J. T. Anderson, L. Golenstani-Rad, and S. J. Graham, 'Investigation of Parallel Radiofrequency Transmission for the Reduction of Heating in Long Conductive Leads in 3 Tesla Magnetic Resonance Imaging', *PLOS ONE*, vol. 10, no. 8, p. e0134379, Aug. 2015.

[8] F. Settecase *et al.*, 'RF Heating of MRI-Assisted Catheter Steering Coils for Interventional MRI', *Acad. Radiol.*, vol. 18, no. 3, pp. 277–285, Mar. 2011.

[9] S. Fandrey, S. Weiss, and J. Müller, 'A novel active MR probe using a miniaturized optical link for a 1.5-T MRI scanner', *Magn. Reson. Med.*, vol. 67, no. 1, pp. 148–155, 2012.

[10] Y. S. Yaras *et al.*, 'Acousto-Optic Catheter Tracking Sensor for Interventional MRI Procedures', *IEEE Trans. Biomed. Eng.*, vol. 66, no. 4, pp. 1148–1154, Apr. 2019.

[11] J. L. Edmunds, S. Sonmezoglu, and M. M. Maharbiz, 'Piezoelectric-based optical modulator for miniaturized wireless medical implants', *Opt. Express*, vol. 30, no. 24, pp. 43664–43677, Nov. 2022.

[12] J. L. Edmunds, S. Sonmezoglu, J. Martens, A. Von Meier, and M. M. Maharbiz, 'Optical voltage sensor based on a piezoelectric thin film for grid applications', *Opt. Express*, vol. 29, no. 21, p. 33716, Oct. 2021.

[13] K. Möllenhoff, A.-M. Oros-Peusquens, and N. J. Shah, 'Introduction to the Basics of Magnetic Resonance Imaging', in *Molecular Imaging in the Clinical Neurosciences*, G. Gründer, Ed., Totowa, NJ: Humana Press, 2012, pp. 75–98.

CONTACT

*Alp A. Derin: derin.a@northeastern.edu
*Soner Sonmezoglu; s.sonmezoglu@northeastern.edu